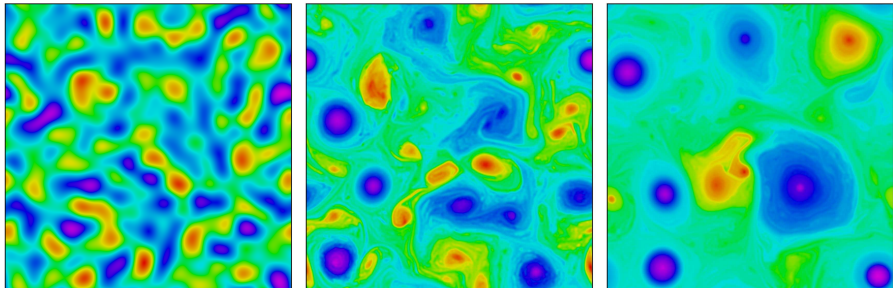


# Balance, and imbalance in complex nonlinear geophysical and astrophysical flows



David Dritschel  
University of St Andrews  
November 2024

- 1 Diagnosing balance and imbalance
  - Balance relations
  - PV inversion
- 2 Hydrostatic and non-hydrostatic shallow-water models revisited
  - Conservation
  - Numerical methods
  - Linear waves
  - Discussion
- 3 3D non-hydrostatic rotating stratified flows
  - Re-casting the equations of motion
  - Nonlinear QG balance
  - Optimal PV balance
- 4 An application to shallow-water MHD
- 5 Conclusions

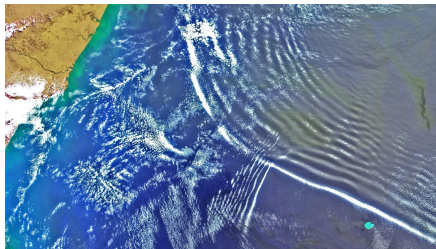
# Balance and imbalance in geophysical fluid dynamics

Atmospheric and oceanic flows often exhibit *relations* between fields, indicating that some terms in the governing equations are *sub-dominant*.

For example,

- *hydrostatic balance* implies the *vertical* acceleration is *negligible*;
- *geostrophic balance* implies the *horizontal* acceleration is *negligible*.

Such balances are used to construct the *quasi-geostrophic* (balance) model. We *lose two time derivatives* and *filter* relatively high-frequency *inertia-gravity waves*.



# Balance and imbalance in geophysical fluid dynamics

The justification is that inertia–gravity waves tend to be **energetically weak** compared to the **slow, ponderous** balanced flow.

**However**, other **potentially more accurate** balance relations may be sought — ones that make the residual *imbalance* weaker.

**For example**, for a shallow water flow in **height-velocity variables**  $(h, u, v)$ , these relations take the form

$$F(h, u, v) = 0 \quad \& \quad G(h, u, v) = 0$$

where  $F$  and  $G$  may be nonlinear differential operators. The definition of **potential vorticity**  $q$  **provides a further relation** to determine  $h$ ,  $u$ , and  $v$  entirely from  $q$ , **the 'master variable'** (chosen since  $Dq/Dt = 0$ ).

**Hierarchies** of such relations exist, whose accuracy depends on **Rosby** and **Froude** numbers (Mohebalhojeh & Dritschel, *J. Atmos. Sci.* 2001).

# Examples of balance relations

The QG model uses the *simplest* balance relations

$$\delta = \nabla \cdot \mathbf{u} = 0 \quad \& \quad \gamma = f \nabla^\perp \cdot \mathbf{u} - g \nabla^2 h = 0$$

where  $\nabla^\perp \cdot \mathbf{u} = \zeta$ , the relative vorticity. Thus, the flow is **non-divergent** and **geostrophic**:  $\gamma$  here is the **ageostrophic vorticity (times  $f$ )**.

A **substantially more accurate balance**, used below, instead uses  $\partial\delta/\partial t = 0$  and  $\partial\gamma/\partial t = 0$ , leading to

$$\gamma + 2J(u, v) - \nabla \cdot (\delta \mathbf{u}) = 0 \quad \& \quad g \nabla^2 (\nabla \cdot (h \mathbf{u})) - f \nabla \cdot ((\zeta + f) \mathbf{u}) = 0.$$

These relations, **together with the definition of PV**  $q = H(h, u, v)$ , e.g.

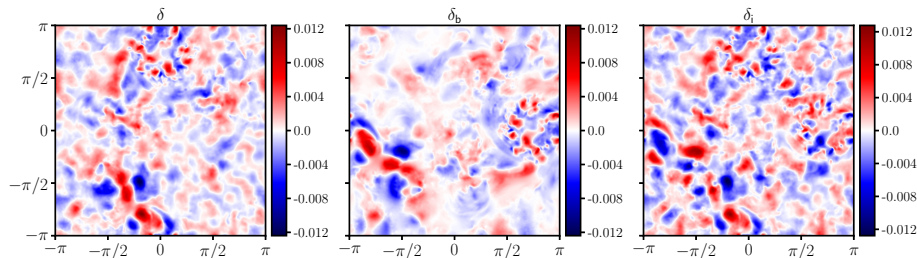
$$q = \frac{\zeta + f}{h},$$

enable one to recover  $h$ ,  $u$  and  $v$  from  $q(\mathbf{x}, t)$ , **at each instant of time**  $t$ .

# Examples of balance relations

When used to diagnose balance, the **balanced** fields thus obtained are subscripted “b”, i.e.  $h_b$ ,  $u_b$  and  $v_b$ .

The **imbalanced** fields are the differences from the **original fields**, i.e..  
 $h_i = h - h_b$ ,  $u_i = u - u_b$  and  $v_i = v - v_b$ .



In practice, the original fields are those computed **in a particular shallow-water (SW) flow simulation**.

# Potential vorticity and inversion

Potential vorticity (PV) conservation in an **adiabatic**, **inviscid** flow is a consequence of **Kelvin's circulation theorem**.

The special status of PV as a **nearly** conservative tracer is **immensely useful** for understanding atmospheric and oceanic dynamics.

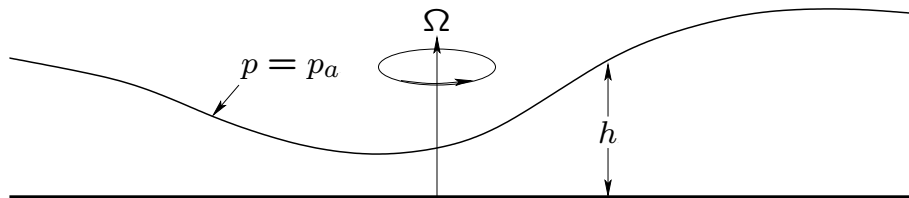
**Combined with balance**, PV allows one to **diagnose** both dynamical and thermodynamical fields by 'PV inversion' (**Hoskins, McIntyre & Robertson, *Quart. J. Roy. Meteorol. Soc.* 1985**).

It **also** allows one to diagnose the residual **imbalance**, the “inertia–gravity waves”.

Here we study this imbalance **first** in a **non-hydrostatic** (and ageostrophic) shallow-water model, **then** in the **fully three-dimensional** “parent” model.

# The shallow-water model

The **hydrostatic** shallow-water originated in the 19<sup>th</sup> century (Saint-Venant, 1871), and has been used extensively ever since.



It is a **long-wave** theory, where horizontal scales  $L$  are assumed **large** compared to the depth  $h$ . Further, the **hydrostatic** approximation is made, **and** the horizontal velocity  $\mathbf{u}$  is assumed to be **independent of height**  $z$ .

# The non-hydrostatic shallow-water model

Green & Naghdi (1976) derived a more accurate model by relaxing the hydrostatic approximation while retaining the height-independence of  $\mathbf{u}$  (historically Serre, 1953 derived the equations first, see Dritschel & Jalali, *JFM* 2020).

This model allows one to more reliably model shorter scales ( $L < h$ ), which are fundamentally *non-hydrostatic*.

---

Here we explore how this affects the evolution of rotating shallow-water turbulence, in particular the excitation of inertia–gravity waves.

The non-hydrostatic equations are derived by vertically-averaging the 3D parent system (see D & J, 2020), assuming only  $\mathbf{u}$  is independent of  $z$ .

We therefore refer to this model as the Vertically-Averaged (VA) model.

The VA model conserves **potential vorticity (PV)** on fluid particles

$$\frac{Dq}{Dt} = 0, \quad q = \frac{\zeta + f}{h} + \frac{1}{3}J(h, \delta)$$

besides global invariants like energy, linear and angular momentum (depending on boundary conditions).

---

Computationally, we use **Contour Advection** to accurately model PV conservation (Dritschel & Fontane, J. Comput. Phys. 2010).

*To also accurately model the wave motions*, we re-cast the equations and explicitly evolve  $q$ ,  $\delta = \nabla \cdot \mathbf{u}$  and  $\gamma = f\zeta - g\nabla^2 h$  (ageostrophic vorticity), see Mohebalhojeh & D (2000).

# Inversion

The use of  $q$ ,  $\delta$  and  $\gamma$  entails solving a series of **linear, elliptic** problems. This is **necessary** to preserve the **underlying balance**. Otherwise, **spurious** inertia–gravity waves are generated by numerical inaccuracies.

First of all, we use a **Helmholtz decomposition** for the velocity field:

$$\mathbf{u} = -\frac{\partial\psi}{\partial y} + \frac{\partial\chi}{\partial x} \quad \& \quad \mathbf{v} = \frac{\partial\psi}{\partial x} + \frac{\partial\chi}{\partial y}.$$

Here,  $\psi$  is the **streamfunction** and  $\chi$  is the **divergence potential**.

Then  $\chi$  is determined **directly** from the definition of  $\delta$ :  $\nabla^2\chi = \delta$ . It is **prudent** to use the **dimensionless height anomaly**

$$\tilde{h} = \frac{h - H}{H}$$

where  $H$  is the constant mean depth (**due to mass conservation**).

# Inversion

It is **also** prudent to use the **re-scaled PV anomaly**

$$\tilde{q} = \frac{\zeta + f}{1 + \tilde{h}} - f$$

— it still follows that  $D\tilde{q}/Dt = 0$  (for constant  $f$ ).

From the definition of  $\tilde{q}$ , **and the Helmholtz decomposition**, we have

$$\nabla^2 \psi = \zeta = (f + \tilde{q})(1 + \tilde{h}) - f = \tilde{q} + (f + \tilde{q})\tilde{h}.$$

**However**, we don't yet know  $\tilde{h}$ . But the definition of  $\gamma \Rightarrow$

$$\gamma = f\zeta - c^2 \nabla^2 \tilde{h} = f[\tilde{q} + (f + \tilde{q})\tilde{h}] - c^2 \nabla^2 \tilde{h}.$$

Re-arranging this, we obtain a **linear, elliptic** equation for  $\tilde{h}$ :

$$c^2 \nabla^2 \tilde{h} - f(f + \tilde{q})\tilde{h} = f\tilde{q} - \gamma.$$

In summary,

- We find  $\tilde{h}$  for given  $\tilde{q}$  and  $\gamma$ .
- We find the relative vorticity  $\zeta = \tilde{q} + (f + \tilde{q})\tilde{h}$  from  $\tilde{q}$  and  $\tilde{h}$ .
- We find  $\psi$  by inverting  $\nabla^2\psi = \zeta$ .
- We find  $\chi$  by inverting  $\nabla^2\chi = \delta$ .
- We find  $u$  &  $v$  by differentiating  $\psi$  and  $\chi$ .

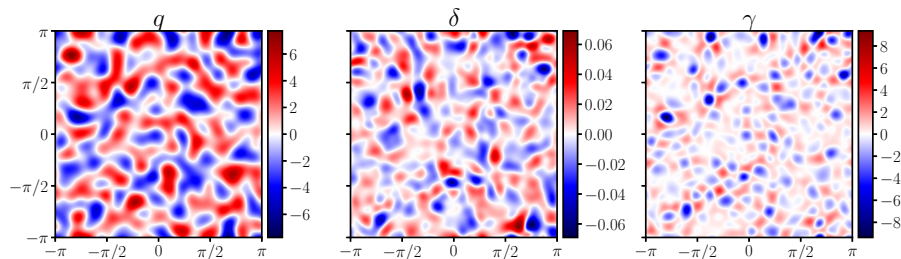


In this way, we obtain the **original primitive** variables  $\tilde{h}$ ,  $u$  and  $v$  from the **re-cast variables**  $\tilde{q}$ ,  $\delta$  and  $\gamma$ .

# Numerical methods (Contour Advection)

- We evolve the *same variables*,  $\tilde{q}$ ,  $\delta$  &  $\gamma$ , in (hydrostatic) SW and VA.
- Doubly-periodic *pseudo-spectral* treatment of  $\delta$  and  $\gamma$  with standard '2/3 rule' to de-alias and *weak*  $\nu \nabla^6$  hyper-diffusion.
- *Semi-implicit* time-stepping for  $\delta$  and  $\gamma$  with built in hyper-diffusion. The iterated trapezoidal rule (Crank-Nicolson) is used for all prognostic variables.
- Basic grid resolution:  $512^2 \Rightarrow$  Effective resolution:  $8192^2$ .
- Domain dimensions  $L_x = L_y = 2\pi$ . Coriolis frequency  $f = 4\pi$ . Rossby deformation length  $L_D = k_D^{-1} = c/f$  specified, where  $c = \sqrt{gH}$  and  $H$  is the mean depth.

# Initial conditions for $k_0 = k_D = 6$ and $H = 0.4$

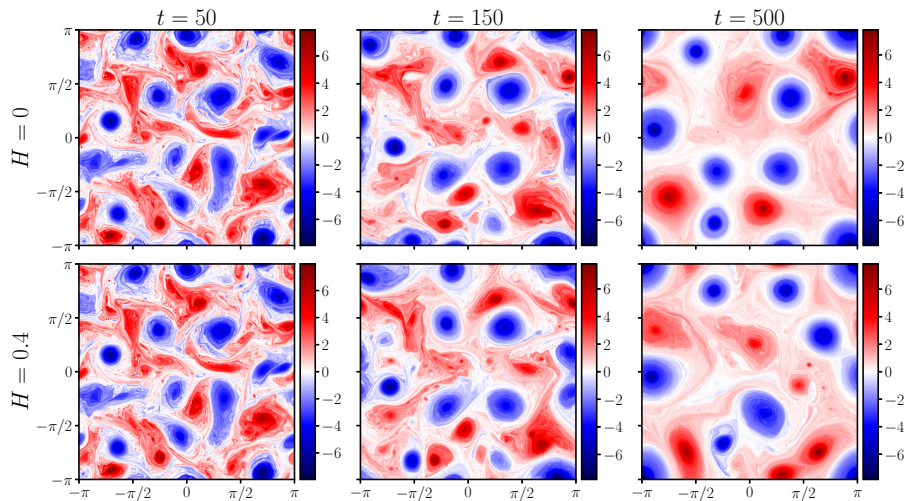


The PV is specified from the spectrum  $k^5 \exp(-2k^2/k_0^2)$ . The Rossby number  $\text{Ro} = H|\tilde{q}|_{\max}/f = 0.6$ . All other initial fields are found by the [balance relations](#)  $p_n = \partial\delta/\partial t = \partial\gamma/\partial t = 0 \Rightarrow$

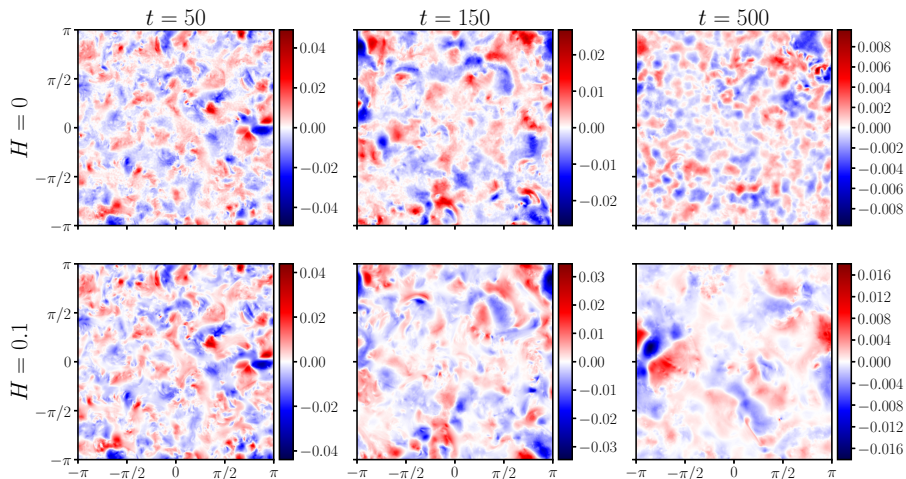
$$\gamma + 2J(u, v) - \nabla \cdot (\delta \mathbf{u}) = 0 \quad \& \quad g\nabla^2(\nabla \cdot (h\mathbf{u})) - f\nabla \cdot ((\zeta + f)\mathbf{u}) = 0$$

— which must be supplemented by the definition of PV.

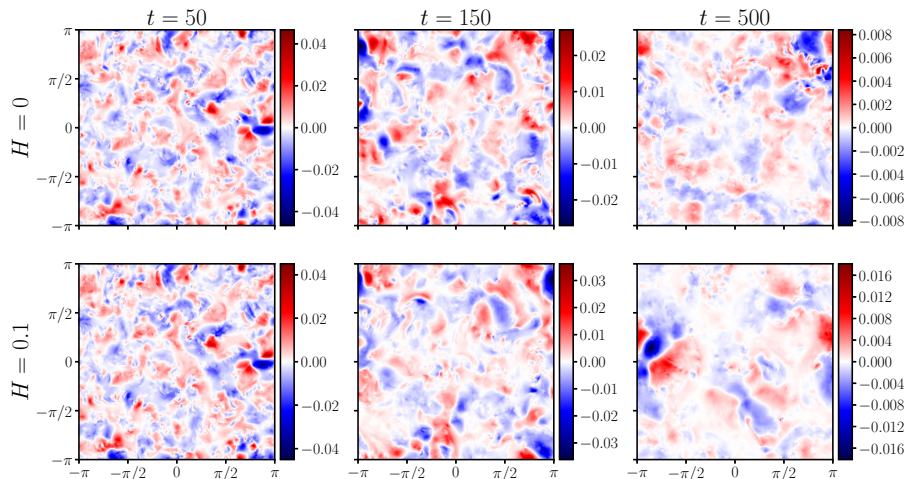
# Flow evolution: PV anomaly, comparing $H = 0$ & $H = 0.4$



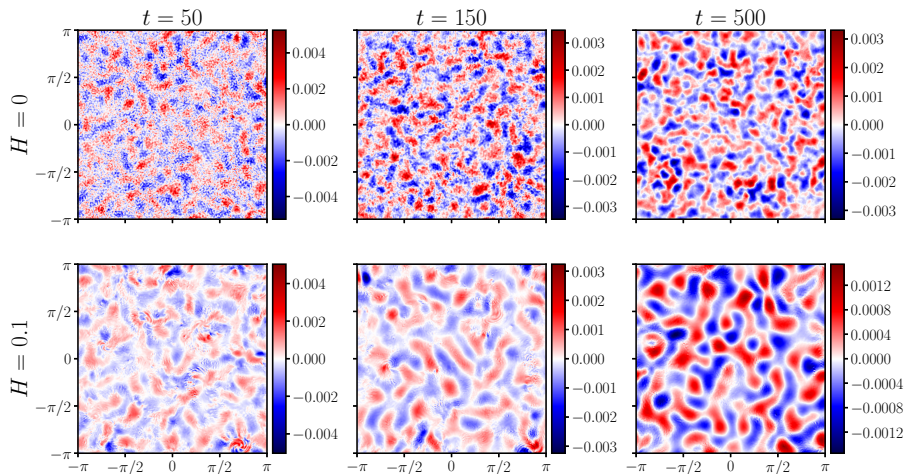
# Evolution of divergence $\delta$ , comparing $H = 0$ & $H = 0.1$



# Evolution of balanced divergence $\delta_b$

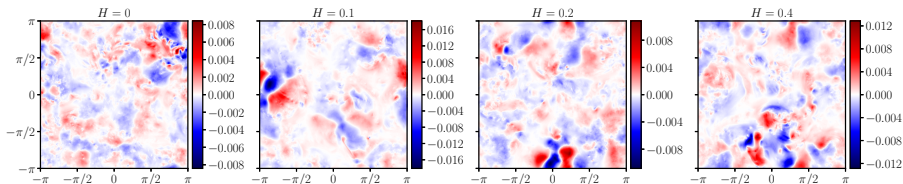


# Evolution of imbalanced divergence $\delta_i = \delta - \delta_b$

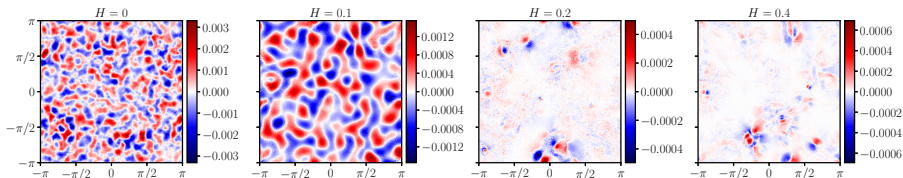


# *balanced* and *imbalanced* divergence at $t = 500$ , varying $H$

$\delta_b$



$\delta_i = \delta - \delta_b$



# Linear waves

In **primitive** variables  $h$ ,  $u$  and  $v$ , the **non-hydrostatic** shallow-water (VA) equations are

$$\frac{D\mathbf{u}}{Dt} + f\mathbf{e}_z \times \mathbf{u} = -\frac{1}{h}\nabla p \quad \text{and} \quad \frac{\partial h}{\partial t} + \nabla \cdot (h\mathbf{u}) = 0$$

where  $p = gh^2/2 + p_n$  is the **vertically-integrated** pressure, while the **non-hydrostatic** part  $p_n$  satisfies the **linear, elliptic** equation

$$\nabla \cdot \left( \frac{\nabla p_n}{h} \right) - \frac{3p_n}{h^3} = \tilde{\gamma},$$

where

$$\tilde{\gamma} \equiv f\zeta - g\nabla^2 h + 2J(u, v) - 2\delta^2$$

is known **entirely** in terms of  $h$ ,  $u$  and  $v$ , where above

$$\delta = \frac{\partial u}{\partial x} + \frac{\partial v}{\partial y} \quad \text{and} \quad \zeta = \frac{\partial v}{\partial x} - \frac{\partial u}{\partial y}.$$

Linearising the VA equations about a state of rest and a mean depth  $H$ , one obtains

$$\frac{\partial \mathbf{u}'}{\partial t} + f \mathbf{e}_z \times \mathbf{u}' = -g \nabla h' - \frac{1}{H} \nabla p'_n \quad \text{and} \quad \frac{\partial h'}{\partial t} + H \nabla \cdot \mathbf{u}' = 0$$

where primes denote perturbation quantities, together with

$$\nabla^2 p'_n - \frac{3p'_n}{H^2} = H(f\zeta' - g\nabla^2 h').$$

Seeking plane-wave solutions  $\propto \exp(i(\mathbf{k} \cdot \mathbf{x} - \omega t))$ , where  $\mathbf{k}$  is the wavevector and  $\omega$  is the frequency, a bit of algebra (!) yields the dispersion relation

$$\omega^2 = \frac{f^2 + c^2 k^2}{1 + H^2 k^2 / 3}$$

$k = |\mathbf{k}|$  is the wavenumber and  $c = \sqrt{gH}$ .

The familiar hydrostatic shallow-water (SW) dispersion relation

$$\omega^2 = f^2 + c^2 k^2$$

is recovered for  $H \rightarrow 0$  (but  $g \rightarrow \infty$  to keep  $c$  finite).

For  $H > 0$ , notably all frequencies  $|\omega|$  lie between  $f$  and  $N = \sqrt{3}c/H = \sqrt{3g/H}$ , called the 'buoyancy frequency'.

- The phase velocity  $c_p = |\omega|/k$  decreases monotonically with  $k$ .
- The group velocity  $c_g = |\partial\omega/\partial k|$  is given by

$$c_g = \frac{|c^2 - H^2 f^2/3| k}{\sqrt{(f^2 + c^2 k^2)(1 + H^2 k^2/3)^3}}.$$

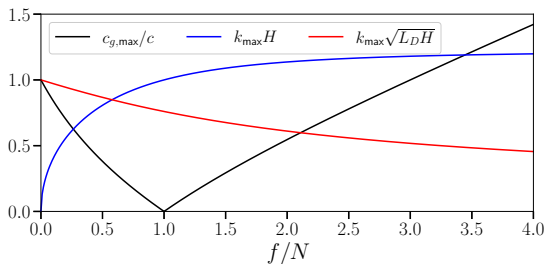
# Group velocity

Alternatively

$$\frac{c_g}{c} = \frac{|1 - \alpha| \kappa}{\sqrt{(3\alpha + \kappa^2)(1 + \kappa^2/3)^3}}$$

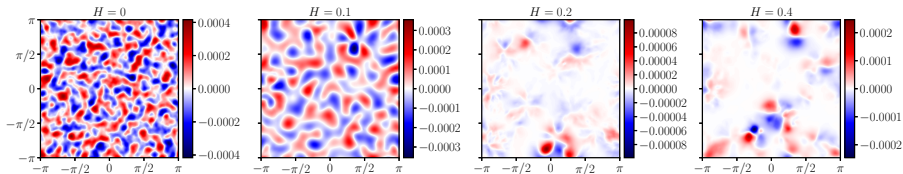
where  $\alpha \equiv (f/N)^2$  and  $\kappa = kH$ . This reaches a maximum when  $\kappa = \sqrt{\sqrt{\alpha^2 + 3\alpha} - \alpha} = k_{\max}H$ .

Moreover, the group velocity *vanishes for all  $k$*  when  $f = N$  ( $\Leftrightarrow \alpha = 1$ ). Then, *linear waves are completely trapped*.

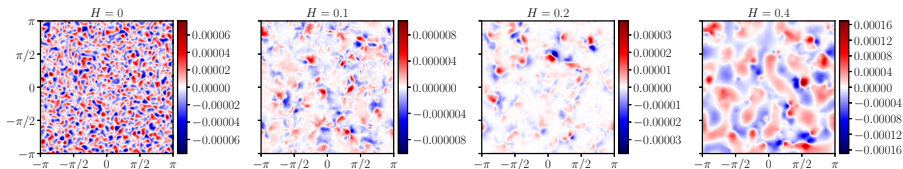


*imbalanced* pressure  $p_i$  at  $t = 500$ , varying  $H$  and  $k_D$

$$k_D = 6 \quad (f/N = 1 \Leftrightarrow H = 0.288\dots)$$

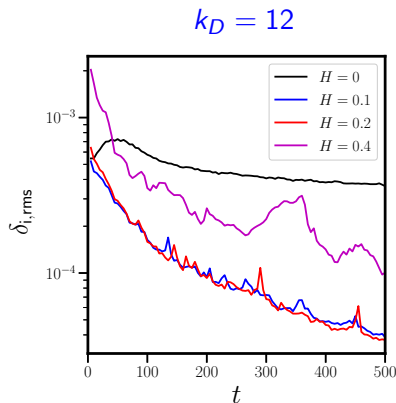
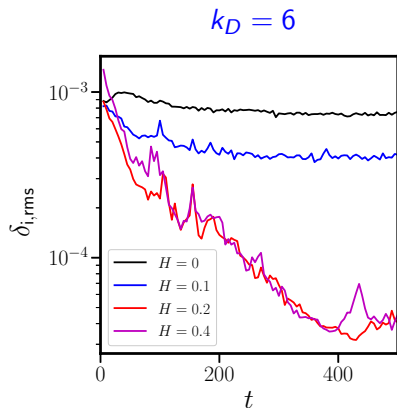


$$k_D = 12 \quad (f/N = 1 \Leftrightarrow H = 0.144\dots)$$



Wave trapping occurs for  $f/N \sim 1$ .

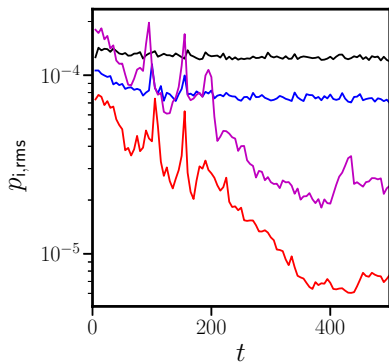
# R.m.s. imbalanced divergence $\delta_i$ versus time



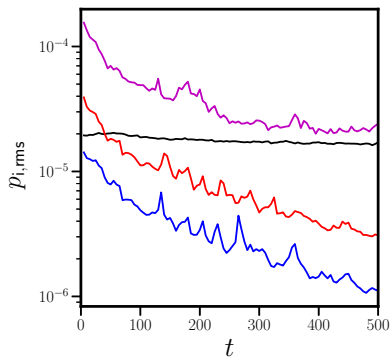
- Minimal imbalance occurs when  $f/N \sim 1$ .

# R.m.s. imbalanced pressure $p_i$ versus time

$k_D = 6$



$k_D = 12$



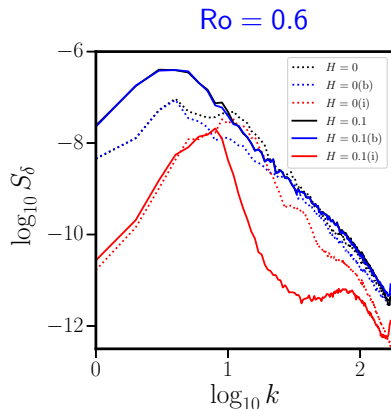
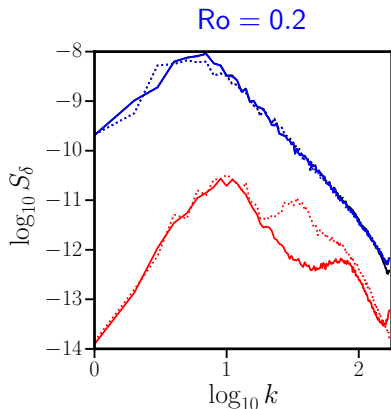
—  $H = 0$

—  $H = 0.1$

—  $H = 0.2$

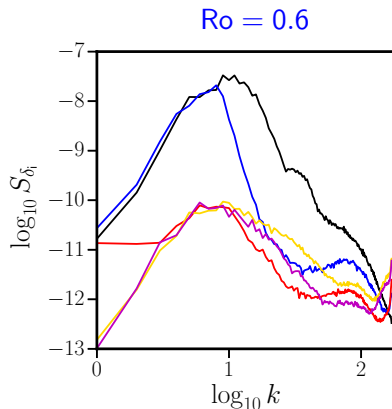
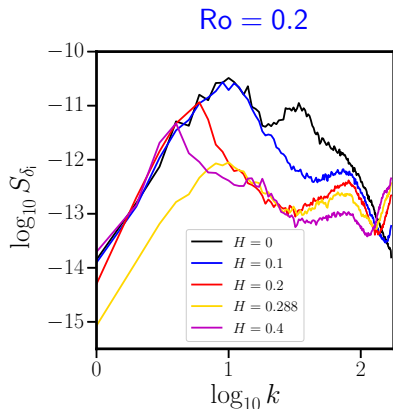
—  $H = 0.4$

# Spatial spectra of divergence $\delta$ at $t = 500$ for $k_D = 6$



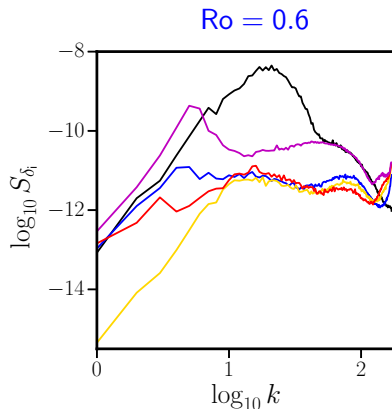
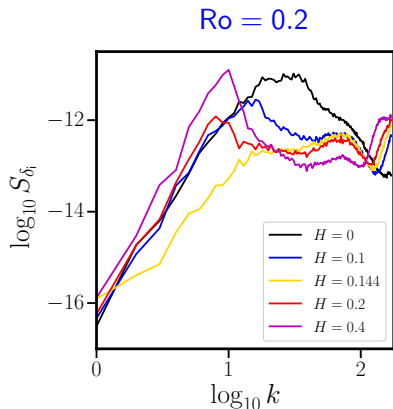
- Even for  $H = 0.1$ , the imbalance is greatly reduced for  $k > \sqrt{3}/H$ , where strong dispersion occurs.

# Spectra of imbalanced divergence $\delta_i$ at $t = 500$ for $k_D = 6$



- The **greatest reduction** in imbalance occurs when  $f/N = 1$  (yellow) and **linear waves** are trapped.

# Same again ... but for $k_D = 12$



- The **greatest reduction** in imbalance occurs when  $f/N = 1$  (yellow) and **linear waves** are trapped.

# Frequency spectra

Recall that the **dispersion relation** for **inertia–gravity waves** on a basic state **at rest** is

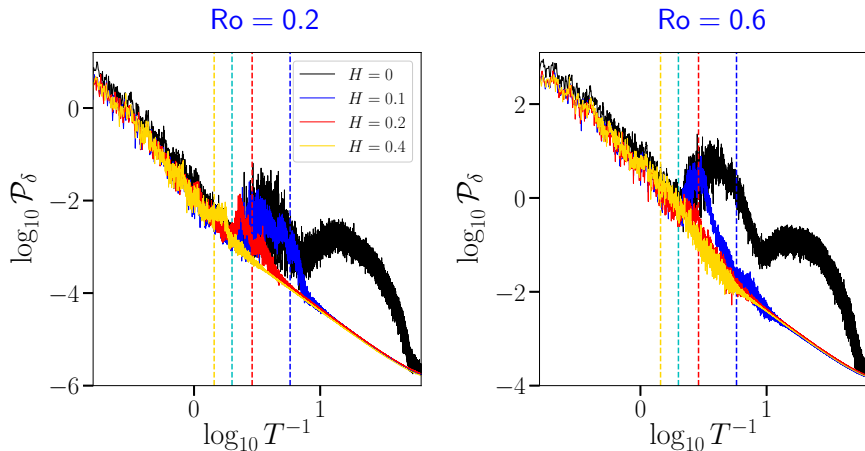
$$\omega^2 = \frac{f^2 + c^2 k^2}{1 + H^2 k^2 / 3} = \frac{f^2 + N^2 \kappa^2 / 3}{1 + \kappa^2 / 3}$$

where  $\kappa = kH$  (the **dimensionless wavenumber**) and  $N = \sqrt{3g/H}$ .

- $\omega \rightarrow f$  as  $\kappa \rightarrow 0$  (long waves)
- $\omega \rightarrow N$  as  $\kappa \rightarrow \infty$  (short waves)

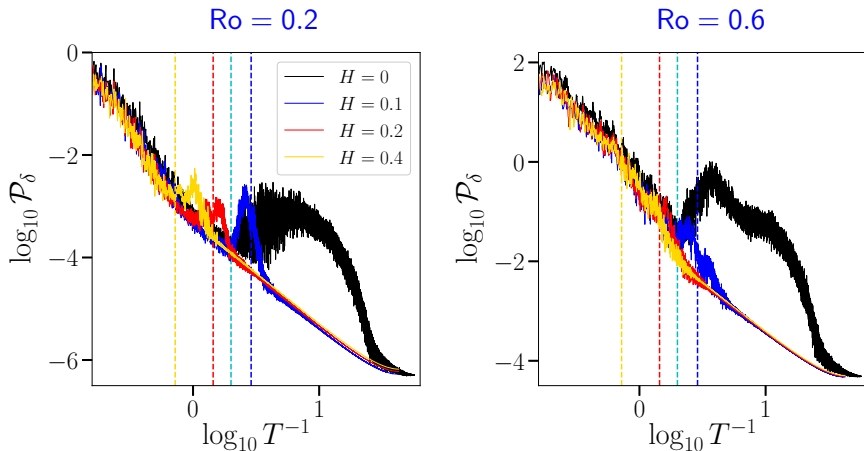
In the simulations, the divergence  $\delta$  was saved at 16 equally-spaced grid points every time step. **Then**, each time series was **Fourier analysed** to create a frequency spectrum. **Finally**, the 16 spectra were averaged into a single spectrum,  $\mathcal{P}_\delta$ .

# Frequency spectra of divergence $\delta$ for $k_D = 6$



- Here,  $T^{-1} = \omega/(2\pi)$  is the **sidereal frequency**.

# Frequency spectra of divergence $\delta$ for $k_D = 12$



- The **vertical lines** mark  $f$  (cyan) and  $N$  (various  $H$ , other colours)

## Discussion (1/3)

The inclusion of non-hydrostatic effects generally **complicates** the equations of motion.

*However*, such effects **reduce IGW emission** ✓, *and* provide a natural frequency bound ( $N$ ) **useful for limiting the time step**  $\Delta t \sim N^{-1}$  ✓.

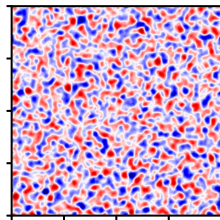
**Counter-intuitively**, relaxing hydrostatic balance leads to more balance!

In a rotating stratified flow, the key parameter is the **Coriolis–buoyancy** frequency ratio  $f/N$ .

(Recall  $N = \sqrt{3c/H} = \sqrt{3g/H}$  in the SW model.)

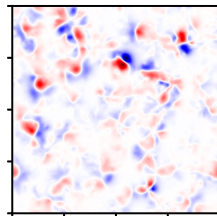
- When  $f/N \ll 1$ , non-hydrostatic effects are weak — **except at very small scales**  $L \sim H$ .

IGWs tend to be small-scale and widely dispersed.

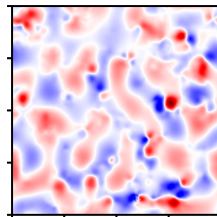


## Discussion (2/3)

- When  $f/N \sim 1$ , non-hydrostatic effects **strongly suppress** IGWs and trap the waves near **intense** circulation regions — **predominantly anti-cyclones**.



- When  $f/N \gg 1$ , **waves are no longer trapped** but spread throughout the domain. **IGWs tend to be large-scale**.



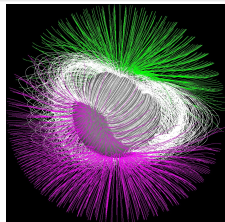
## Discussion (3/3)

Commonly,  $f/N \ll 1$  in the atmosphere  $\sim 10^{-2}$  and oceans  $\sim 10^{-1}$ .

However, there are exceptions. These occur in regions of weak stratification, e.g. the Western Mediterranean, polar oceans, estuaries, etc. Other planetary atmospheres (and oceans)?

While idealised, a single-layer non-hydrostatic model is convenient for re-assessing fundamental processes in geophysical fluid dynamics.

Moreover, it is readily extendible to include bottom topography (with Ted Johnson, Reza & Mahdi Jalali), as well as magnetic fields, providing a new approach to modelling the solar 'tachocline' and 'hot Jupiter' exoplanets (Dritschel & Tobias, JFM **973**, A17, 2023).



# 3D non-hydrostatic rotating stratified flows

More realistic 3D flows are often modelled by the Oberbeck–Boussinesq equations:

$$\frac{D\mathbf{u}}{Dt} + 2\boldsymbol{\Omega} \times \mathbf{u} = -\frac{\nabla p}{\rho_0} + b\hat{\mathbf{e}}_z, \quad \frac{Db}{Dt} = 0, \quad \nabla \cdot \mathbf{u} = 0,$$

where  $\mathbf{u} = (u, v, w)$  is the velocity,  $p$  is the pressure,  $\rho_0$  is the (constant) background density, and  $b = -g(\rho - \rho_0)/\rho_0$  is the buoyancy.

- Here, we take the background rotation  $\boldsymbol{\Omega} = (0, 0, f/2)$  (upward).

As written, these equations *hide* PV conservation. But, since  $b$  is materially conserved, it follows that the PV

$$q = \boldsymbol{\omega}_a \cdot \nabla b = (\boldsymbol{\omega} + f\mathbf{e}_z) \cdot \nabla b$$

is also materially conserved.

This motivates using the PV as a prognostic variable, i.e.  $Dq/Dt = 0$ , but then what equation(s) do we replace?

# Re-casting the equations of motion

Dritschel & Viúdez, *JFM* **488** (2003) proposed replacing the full set  $\mathbf{u}$  &  $b$  by  $\mathbf{A}_h$  &  $q$ , where

$$\mathbf{A} = \frac{\boldsymbol{\omega}}{f} + \frac{\nabla b}{f^2}$$

where  $\mathbf{A}_h$  denotes 'the horizontal part' of  $\mathbf{A}$ .

The variable  $\mathbf{A}_h$  represents the departure from 'thermal-wind balance' (i.e. hydrostatic–geostrophic balance), which is normally written

$$f \frac{\partial u}{\partial z} = -\frac{\partial b}{\partial y} \quad \text{and} \quad f \frac{\partial v}{\partial z} = \frac{\partial b}{\partial x}.$$

However, the  $x$  and  $y$  components of  $\boldsymbol{\omega} = \nabla \times \mathbf{u}$  are

$$\xi = \frac{\partial w}{\partial y} - \frac{\partial v}{\partial z} \quad \text{and} \quad \eta = \frac{\partial u}{\partial z} - \frac{\partial w}{\partial x}.$$

Hence,  $\mathbf{A}_h = 0$  corresponds to thermal-wind balance upon neglecting  $\nabla_h w$ , i.e.  $f\boldsymbol{\omega}_h \approx -\nabla_h b$ .

# Re-casting the equations of motion

The prognostic equations for the re-cast system are, equivalently,

$$\frac{Dq}{Dt} = 0, \quad \frac{D\mathbf{A}_h}{Dt} + f\mathbf{e}_z \times \mathbf{A}_h = \frac{1}{f}(\boldsymbol{\omega} \cdot \nabla)\mathbf{u}_h + (1 - \sigma^{-2})\nabla_h W - \frac{1}{f^2}(\nabla_h \mathbf{u}) \cdot \nabla b'$$

where  $b'$  is the buoyancy anomaly defined through

$$b = N^2 z + b',$$

$N$  is the buoyancy frequency (constant), and  $\sigma = f/N$ , which is typically small in the atmosphere and oceans. (Note:  $c = N/f = \sigma^{-1}$  below.)

Unlike the original system, one now must recover the original variable  $\mathbf{u}$  &  $b'$  by inversion, i.e. by solving a set of elliptic problems. Introducing a vector potential  $\boldsymbol{\varphi} = (\varphi, \psi, \phi)$  in terms of which  $\mathbf{A} = \nabla^2 \boldsymbol{\varphi}$ , it follows that

$$\mathbf{u} = -f\nabla \times \boldsymbol{\varphi} \quad \text{and} \quad b' = f^2 \nabla \cdot \boldsymbol{\varphi}.$$

# Re-casting the equations of motion

The vector potential is **itself** recovered by solving the *elliptic inversion problems*

$$\nabla^2 \varphi_h = \mathbf{A}_h,$$

**first** for  $\varphi_h$ , **then**

$$\mathcal{L}\phi = \varpi + (1 - \sigma^2) \frac{\partial \Theta}{\partial z} - \sigma^2 \mathcal{N}(\varphi),$$

for  $\phi$ . Above,  $\phi$  is the **vertical component** of  $\varphi$ ,

$$\mathcal{L} = \nabla_h^2 + \sigma^2 \frac{\partial^2}{\partial z^2}$$

is the usual **quasi-geostrophic (QG)** inversion operator,  $\varpi = \boldsymbol{\omega} \cdot \nabla b' / fN^2$  is the **dimensionless PV anomaly** (note  $D\varpi/Dt = 0$ ),  $\Theta = \nabla_h \cdot \varphi_h$  and

$$\mathcal{N}(\varphi) = \nabla(\nabla \cdot \varphi) \cdot [\nabla^2 \varphi - \nabla(\nabla \cdot \varphi)].$$

The equation for  $\phi$  is a **double Monge-Ampère** equation **with lots of interesting properties!**

# Re-casting the equations of motion

## Why go to all this trouble?

Re-casting the equations has **two major benefits**:

- Material conservation of PV is explicit; and
- The underlying QG balance is explicit: **as in QG, elliptic inversion problems must be solved.**



Note, the equations are *unapproximated*, just transformed to make the underlying balance explicit.

Such transformations are known to *greatly improve* the ability of numerical simulations to capture *both* the **balanced** and **imbalanced** motions — (Mohebalhojeh & Dritschel, 2000, 2001, 2004, 2007, 2011, 2016; Smith & Dritschel, 2006; Viúdez & Dritschel 2002, 2003, 2004, 2006; Dritschel & Viúdez 2007, *etc.*)

# Rotating stratified turbulence: *a demanding test*

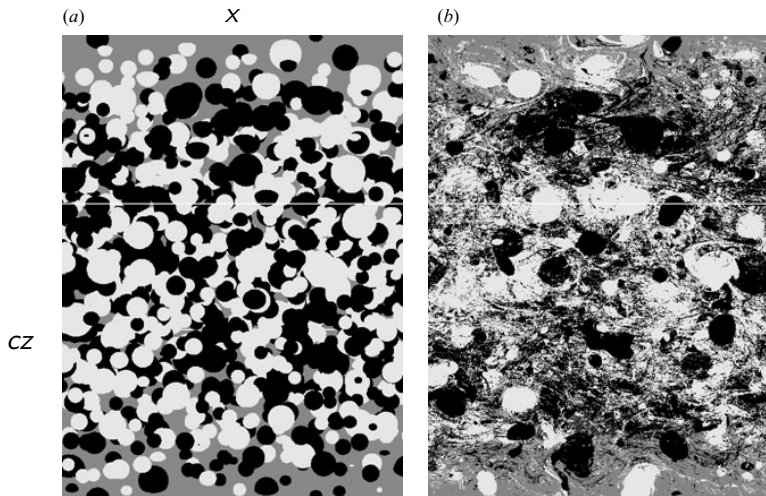


FIGURE 1. Distribution of QG PV anomaly  $q$  at times (a)  $t=0$  and (b)  $t=40$ . The view is orthographic, at an angle of  $60^\circ$  from the vertical, and from the  $(y, z)$ -plane. From this view we can see the top and front faces of the domain and a white line indicates where these faces intersect. Cyclonic vortices are lightly shaded while anticyclonic vortices are darkly shaded.

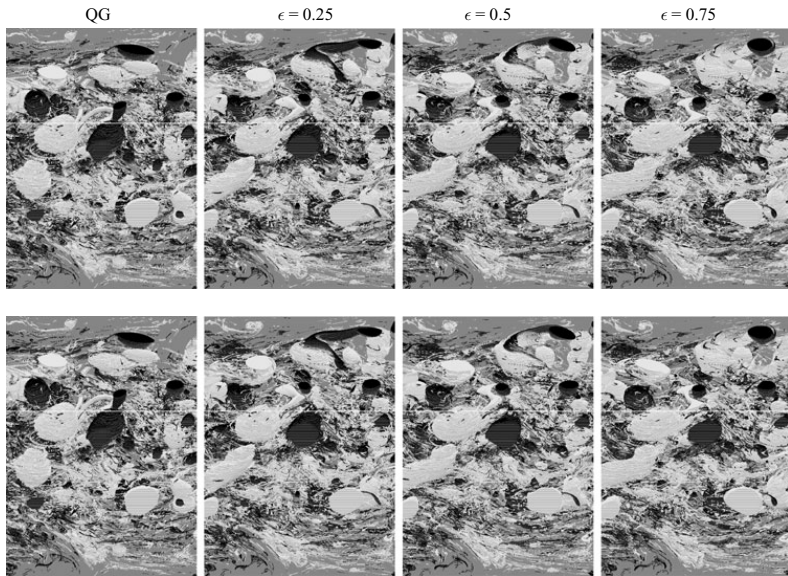


FIGURE 2. Comparison of the PV anomaly fields  $\varpi$  for various PV-based Rossby numbers  $\epsilon$  as labelled, at 5 QG time units. The top row is for  $c=10$  and the bottom row is for  $c=100$ . The view and shading is as in figure 1, but only the inner eighth of the domain is shown.

# Dependence on Rossby number, $\epsilon$

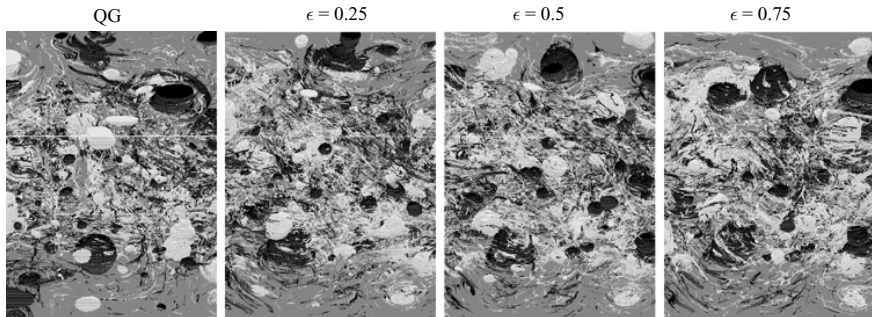


FIGURE 3. Comparison of the QG and NH simulations with  $c = 10$  at time  $t = 20$ . The view and shading is as in figure 2.

**Note:** The Rossby number  $\epsilon$  is the maximum absolute value of the dimensionless PV anomaly  $\varpi$ .

# Diagnosing balance and imbalance

One might anticipate that turbulent flows, with Rossby numbers close to unity, likely contain a significant amount of imbalance, in the form of inertia-gravity waves.

To examine this, we decompose the flow into a balanced component,  $\varphi_b$ , and a residual imbalanced component,  $\varphi_i$ . Note,  $\varphi_i = \varphi - \varphi_b$ .

Alas, there is no exact definition of balance — unless the flow is steady (it is then entirely balanced).

The simplest definition is thermal-wind balance, what we refer to as QG balance. This states that the balanced flow is both geostrophic and hydrostatic. Then,  $\varphi_b = \phi_b \mathbf{e}_z \Rightarrow$  the balanced flow is determined by a scalar potential:  $\mathcal{L}\phi_b = \varpi$ . Moreover,

$$u_b = -f \frac{\partial \phi_b}{\partial y}, \quad v_b = f \frac{\partial \phi_b}{\partial x}, \quad w_b = 0, \quad b'_b = f^2 \frac{\partial \phi_b}{\partial z}.$$

This is just the QG model!

# Nonlinear QG balance

Much more accurate balance conditions exist. An approach **valid to the next order in Rossby number**  $\epsilon$  is 'Nonlinear QG' (NQG) balance, see McKiver & Dritschel, *JFM* **596** (2008).

Here, we take

$$\phi_b = \epsilon\phi_1 + \epsilon^2\phi_2 + \mathcal{O}(\epsilon^3), \quad \varphi_{h,b} = \epsilon^2\varphi_{h2} + \mathcal{O}(\epsilon^3)$$

and **neglect** the  $\mathcal{O}(\epsilon^3)$  terms. The equation for  $\phi_1$  is the same as in QG balance:  $\mathcal{L}\phi_1 = \varpi/\epsilon$ . **Recalling**  $\varphi = (\varphi, \psi, \phi)$ , **at**  $\mathcal{O}(\epsilon^2)$  **one may show**

$$\mathcal{L}\phi_2 - (1 - \sigma^2) \left( \frac{\partial^2 \phi_2}{\partial x^2} + \frac{\partial^2 \psi_2}{\partial x \partial y} \right) = 2\sigma^2 \left( \frac{\partial^2 \phi_1}{\partial z \partial x} \frac{\partial^2 \phi_1}{\partial y^2} - \frac{\partial^2 \phi_1}{\partial x \partial y} \frac{\partial^2 \phi_1}{\partial y \partial z} \right)$$

$$\mathcal{L}\psi_2 - (1 - \sigma^2) \left( \frac{\partial^2 \phi_2}{\partial x \partial y} + \frac{\partial^2 \psi_2}{\partial y^2} \right) = 2\sigma^2 \left( \frac{\partial^2 \phi_1}{\partial x^2} \frac{\partial^2 \phi_1}{\partial y \partial z} - \frac{\partial^2 \phi_1}{\partial x \partial z} \frac{\partial^2 \phi_1}{\partial x \partial y} \right)$$

$$\mathcal{L}\phi_2 - (1 - \sigma^2) \left( \frac{\partial^2 \phi_2}{\partial x \partial z} + \frac{\partial^2 \psi_2}{\partial y \partial z} \right) = 0$$

# Nonlinear QG balance

The equations for the second-order fields  $\varphi_2$  are linear, hence easy to solve in practice.

The procedure is simple:

- Solve  $\mathcal{L}\phi_1 = \varpi/\epsilon$  for  $\phi_1$ . Recall,  $\varpi = \mathcal{O}(\epsilon)$ . Indeed, we define  $\epsilon = |\varpi|_{\max}$  — the *PV-based Rossby number*.
- Compute the derivatives of  $\phi_1$  needed to form the rhs of the linear system above, then invert to find  $\varphi_2$ .

That defines the **balanced** flow,  $\varphi_b$ . The **imbalance** is the residual,  $\varphi_i = \varphi - \varphi_b$ .

Below, the first-order, QG balanced flow is referred to as  $\varphi_{QG}$ , while the second-order, ageostrophic balanced flow is defined by  $\varphi_{AGb} = \varphi_b - \varphi_{QG}$ .

# Optimal PV balance

Perhaps the most **advanced** balancing procedure is 'Optimal PV balance' (OPV balance) (Viúdez & Dritschel, *JFM* **521**, 2004).



**Essentially**, OPV balance seeks the **Lagrangian configuration** of **fluid particles**,  $\tau$  units of time in the past, which **evolve** into the current configuration at  $t = t_0$ , **from a state of rest**, and with PV

$$\varpi(t) = R(t)\varpi(t_0) \quad \text{for} \quad t_0 - \tau \leq t \leq t_0$$

**growing from 0** on each fluid particle:

$$R(t_0 - \tau) = 0 \quad \text{while} \quad R(t_0) = 1.$$

A commonly-used **ramp function** is

$$R(t) = \frac{1}{2} [1 - \cos(\pi(t - t_0 + \tau)/\tau)] .$$

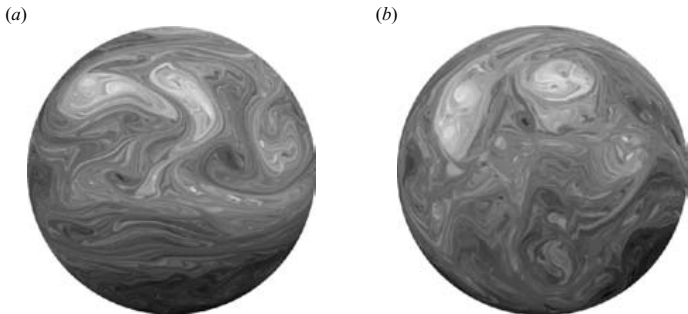


FIGURE 4. (a) The original PV contours,  $\Pi(\mathbf{x}, t)$ , at  $t=10$ , and (b) the PV contours at the beginning of the 4-day ramp,  $\mathbf{r}_{f_6}(\mathbf{X}, t, 0)$ , which evolve into those in (a) from  $\varphi_{f_6}(\mathbf{x}, t, 0) = \mathbf{0}$  while ramping up the PV anomaly. The contours are separated by uniform shades of grey, with an intensity proportional to the PV (white is used for the maximum PV). The actual contours are too dense to plot directly. The view is orthographic from  $0^\circ$  longitude and  $45^\circ$  latitude.

From Viúdez & Dritschel, *JFM* 521, (2004).

# Vertical velocity in a $y = 0$ cross section at $t = 20$

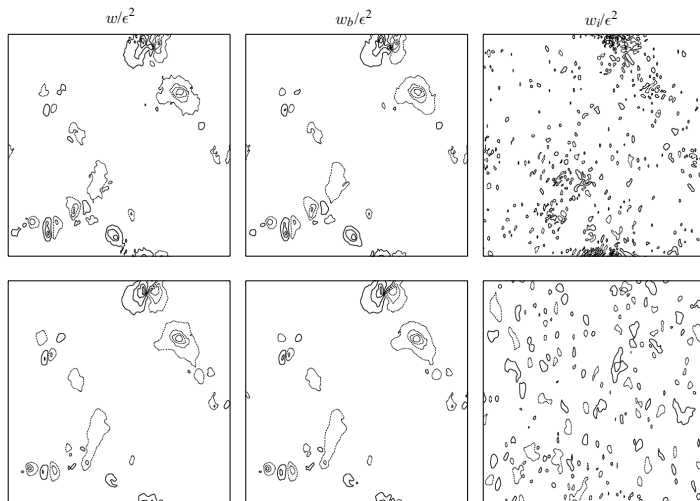


FIGURE 6. Comparison of the full (left column), balanced (middle column) and unbalanced (right column) components of the vertical velocity field at 20 QG time units in a  $y=0$  cross-section for the cases  $c=10$  (top row) and  $c=100$  (bottom row), all with  $\epsilon=0.5$ . The contour intervals for the full, balanced and unbalanced fields are  $\Delta$ ,  $\Delta$  and  $\Delta/4$  where  $\Delta=0.008/c$ .

# Percentage of imbalanced vertical velocity versus time

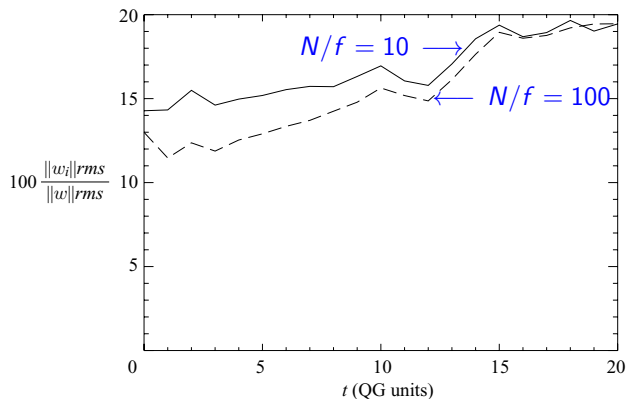
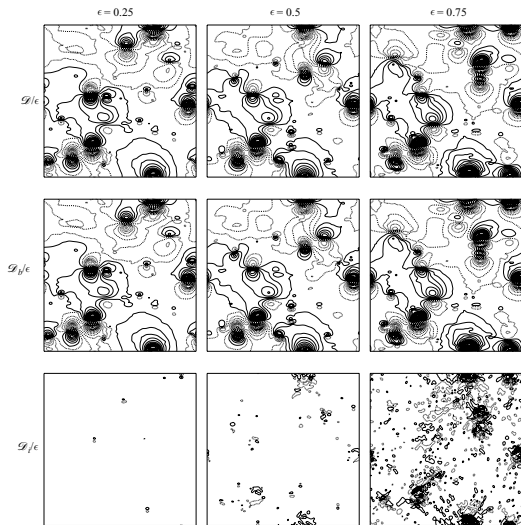


FIGURE 7. Time evolution of the r.m.s. imbalance in  $w$  as a percentage of the total for  $c = 10$  (solid line) and  $c = 100$  (dashed line) when  $\epsilon = 0.5$ .

Even in vertical velocity, the percentage of imbalance remains only a small percentage of the total. The vertical velocity is mostly *balanced*.

# Displacement $-b'/N^2$ in a $y = 0$ cross section at $t = 20$



Three Rossby numbers  $\epsilon$  are compared.

The **imbalance** in this field is a **much smaller fraction** of the total.

FIGURE 8. Comparison of the full (top), balanced (middle) and unbalanced (bottom) components of the displacement field  $\mathcal{D}$  (in a  $y=0$  cross-section) at 20 QG time units for  $c=10$  and for the PV-based Rossby numbers indicated. The contour intervals for the full and balanced fields are  $\Delta=0.008$ . Here, the unbalanced contour interval is 1/50th of the balanced contour intervals.

# Comparison of balancing methods for $-b'/N^2$

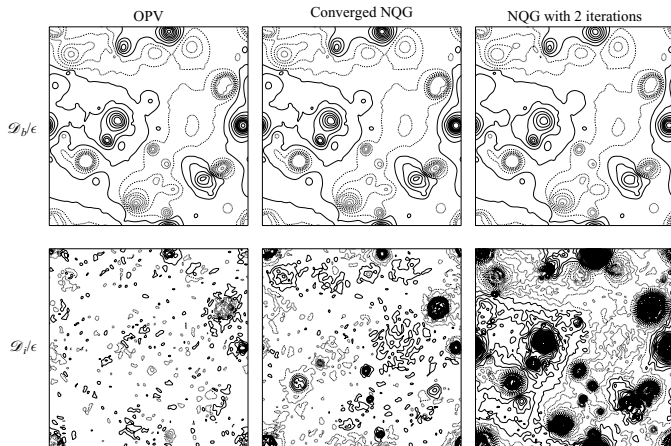
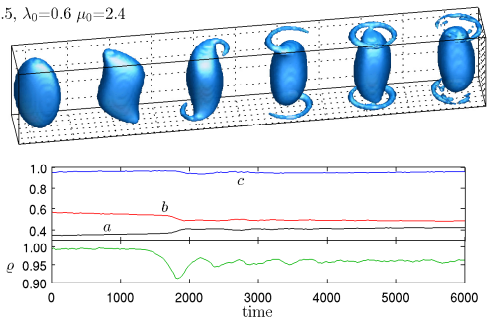


FIGURE 12. Comparison of the balanced (top row) and unbalanced (bottom row) isopycnal displacement obtained using OPV (left column), converged NQG (middle column) and NQG with 2 iterations (right column) — now in a  $z=0$  cross-section—at  $t=20$  time units for  $\epsilon=0.75$ . The balanced contour interval is  $\Delta=0.008$  and the unbalanced contour interval is  $\Delta/50$ .

# A single rotating uniform-PV ellipsoid

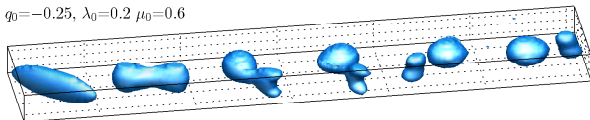
(a)  $q_0=0.5, \lambda_0=0.6, \mu_0=2.4$



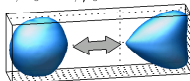
From Tsang & Dritschel *JFM* 762 (2015):

Ellipsoidal vortices in rotating stratified fluids: beyond the quasi-geostrophic approximation

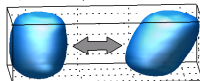
(b)  $q_0=-0.25, \lambda_0=0.2, \mu_0=0.6$



(c)  $q_0=0.25, \lambda_0=0.5, \mu_0=1.4$

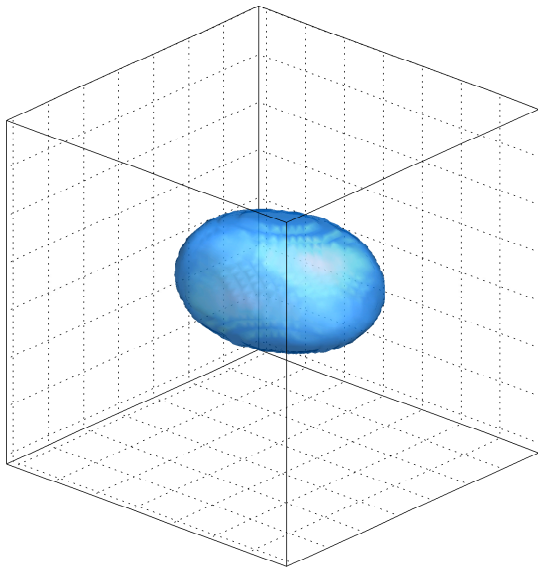


$q_0=-0.5, \lambda_0=0.3, \mu_0=1.0$

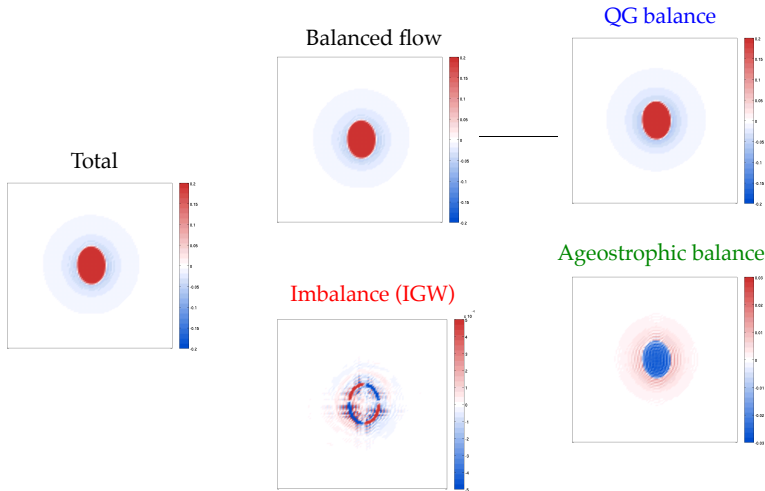


- Here,  $\epsilon = q_0$

# A single rotating uniform-PV ellipsoid



## Balanced and imbalanced components



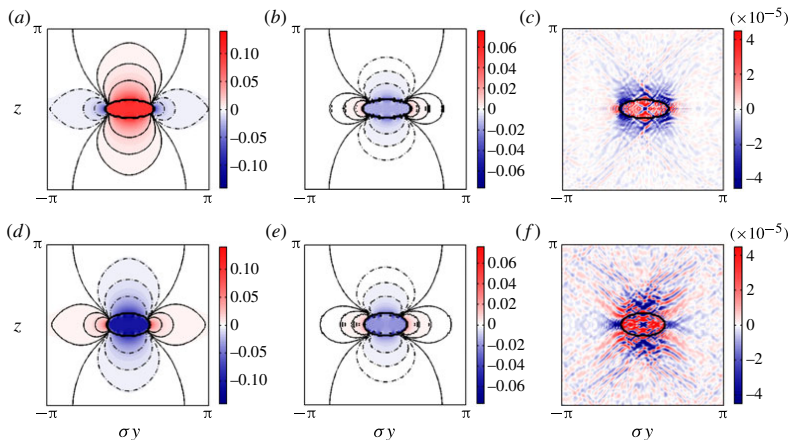
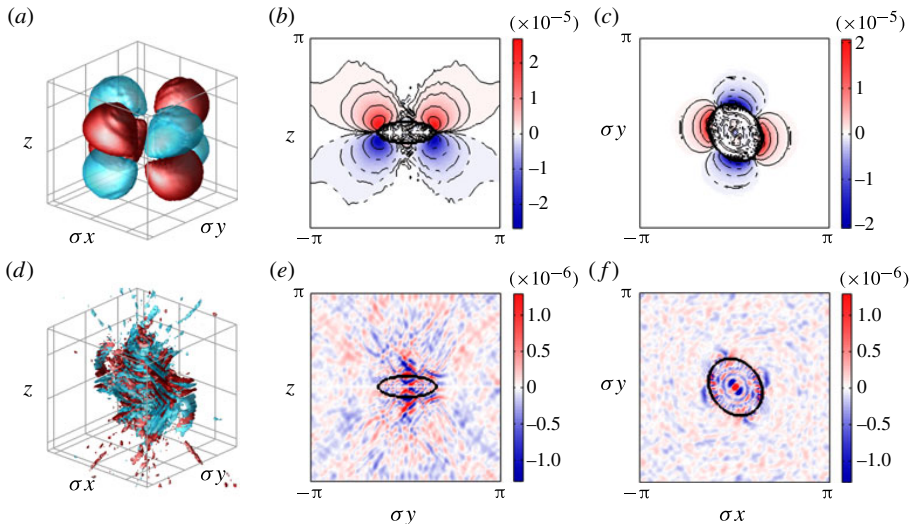


FIGURE 8. (Colour online) A vertical  $y$ - $z$  cross-section at  $x = -\sigma^{-1}\pi/32$  of the scaled vertical vorticity  $\zeta/f$  for a cyclonic vortex or ‘cyclone’ (a–c) and an anticyclonic vortex or ‘anticyclone’ (d–f) with  $q_0 = \pm 0.25$  respectively. The initial aspect ratios are  $\lambda_0 = 0.8$  and  $\mu_0 = 0.4$  in both cases. The QG balanced part  $\zeta_{QG}/f$  is shown in (a) and (d), the

# A single rotating ellipsoid; balance decomposition — $w$



# Energy: quantification of imbalance

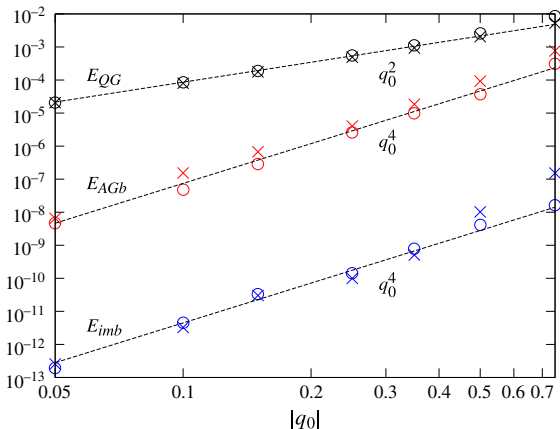
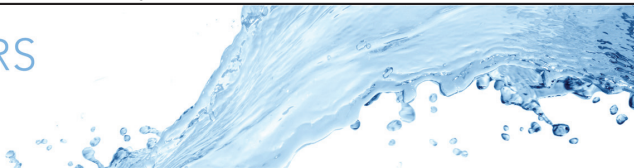


FIGURE 18. (Colour online) Log-log plot of the energy norms for the QG, ageostrophic balanced and imbalanced fields, defined in (5.4), versus the PV-based Rossby number  $q_0$ . Circles represent cyclonic states and crosses anticyclonic states. The initial aspect ratios of the vortex are  $\lambda_0 = 0.3$  and  $\mu_0 = 1.6$ .

*J. Fluid Mech.* (2023), vol. 973, A17, doi:10.1017/jfm.2023.746

**JM** PAPERS



## The magnetic non-hydrostatic shallow-water model

David G. Dritschel<sup>1,†</sup> and Steven M. Tobias<sup>2</sup>

<sup>1</sup>Mathematical Institute, University of St Andrews, St Andrews KY16 9SS, UK

<sup>2</sup>Department of Applied Mathematics, University of Leeds, Leeds LS2 9JT, UK

(Received 16 February 2022; revised 8 June 2023; accepted 5 September 2023)

# Basic equations

Under the **hydrostatic approximation**, the complete set of equations for the **horizontal velocity  $\mathbf{u}$** , magnetic field  $\mathbf{B}$  and **dimensionless height anomaly  $\tilde{h} = (h - H)/H$**  are **momentum**

$$D\mathbf{u} + f \times \mathbf{u} = -c^2 \nabla \tilde{h} + j_z \times \mathbf{B},$$

**induction**

$$D\mathbf{B} - \mathbf{B} \cdot \nabla \mathbf{u} = \eta \nabla^2 \mathbf{B},$$

and **mass**

$$\frac{\partial \tilde{h}}{\partial t} + \nabla \cdot ((1 + \tilde{h})\mathbf{u}) = 0,$$

where  $f$  is the **Coriolis frequency**,  $c^2 = gH$ ,  $g$  is **gravity**,  $H$  is the mean fluid depth,  $j_z$  in the  $z$ -component of the current density, and  $\eta$  is the **magnetic diffusivity**.

# Results: a vortex in a magnetic field

We follow [Dritschel, Diamond & Tobias \(2018\)](#) to study how a magnetic field disrupts a vortex.

Here we study **finite**  $L_D = c/f$  and **shallow-water effects**. **Initially**,

$$\zeta = \frac{\varepsilon f e^{-(r/R)^2/2}}{2(1 - e^{-1/2})} - C$$

with  $f = 4\pi$  and  $R = 5\pi/32$  in a  $[-\pi, \pi]^2$  periodic domain.

**The corresponding maximum velocity**  $U_0 = \frac{1}{2}\omega_0 R$  where  $\omega_0 = \varepsilon f$ .

We take  $\mathbf{B} = (B_x, B_y) = (B_0/(1 + \tilde{h}), 0)$  so that the 3D magnetic field **is tangent to** the upper free surface initially.

We specify  $B_0$  through the 'gain'

$$g \equiv \frac{B_0/\vartheta}{U_0}$$

where  $\vartheta = \Delta x/R$  is the dimensionless diffusion length; note  $\sqrt{\eta/\omega_0} = \Delta x$ .

$B_0/\vartheta$  is the maximum expected magnetic field strength after amplification.

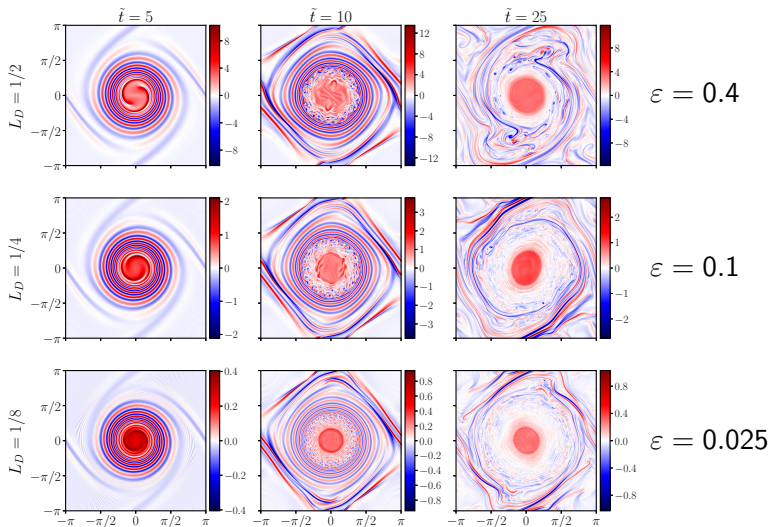
The magnetic Reynolds number

$$\text{Rm} = \frac{U_0 R}{\eta} = \frac{1}{2\vartheta^2}.$$

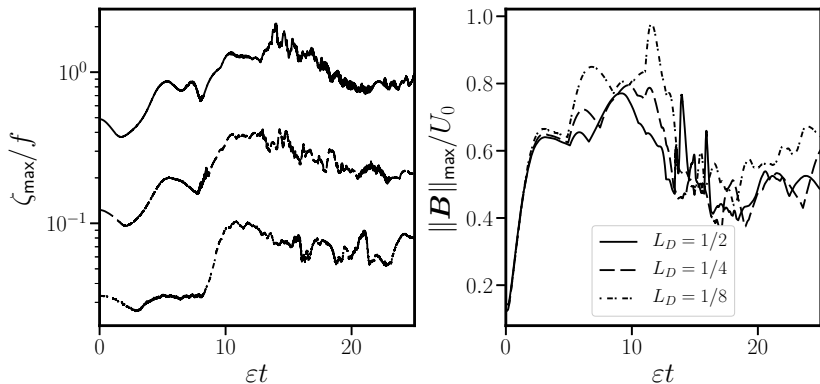
- $\text{Rm} = 800$  at the default grid resolution,  $n_g = 512$ .

# Effect of varying $L_D$ ; $g = 2$

$\zeta(\mathbf{x}, \tilde{t})$  shown. Note  $\varepsilon = 1.6L_D^2$  to keep  $\tilde{h} = \mathcal{O}(1)$  and similar in all cases.

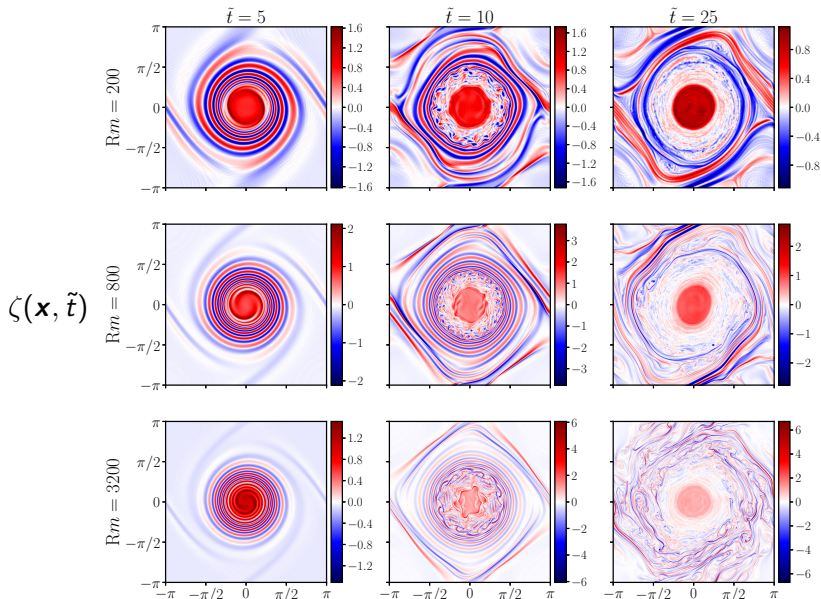


Evolution of the **Rossby number** (left), and **maximum horizontal magnetic field scaled by the maximum flow speed  $U_0$**  (right).

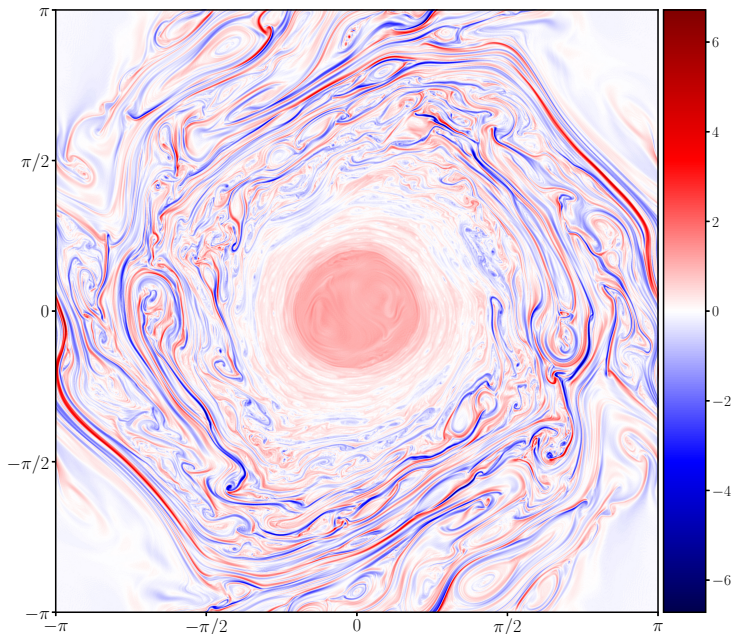


The **actual** gain  $\|B\|_{\max}/U_0$  falls short of the estimate  $g = 2$ .

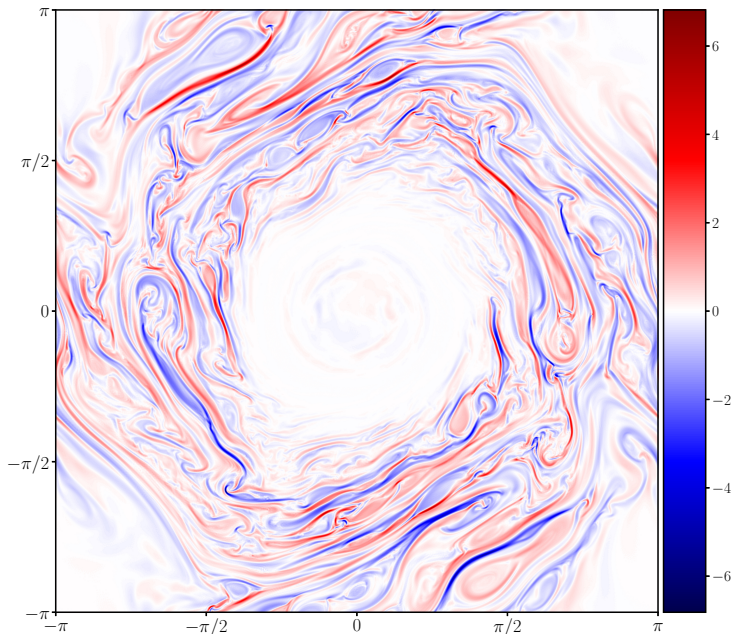
# Effect of varying $Rm$ ; $L_D = 1/4$ , $\varepsilon = 0.1$ , $g = 2$



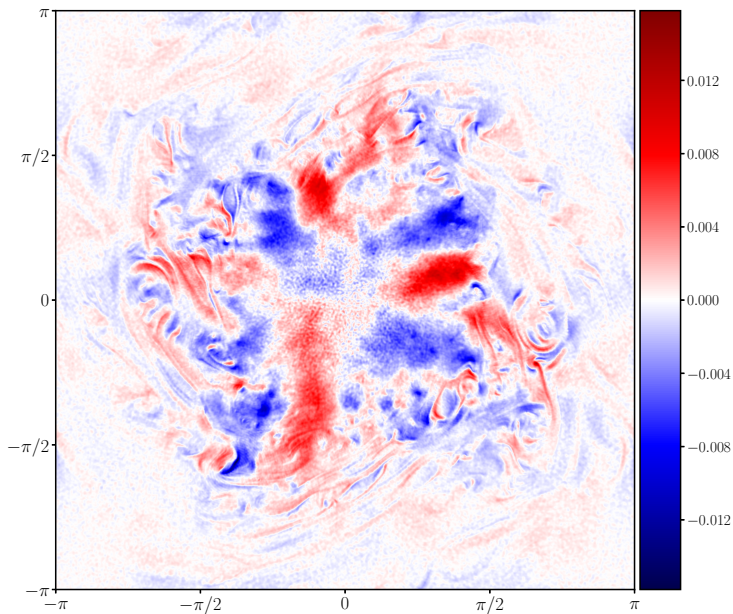
# $\zeta(\mathbf{x}, 25)$ at $\text{Rm} = 3200$



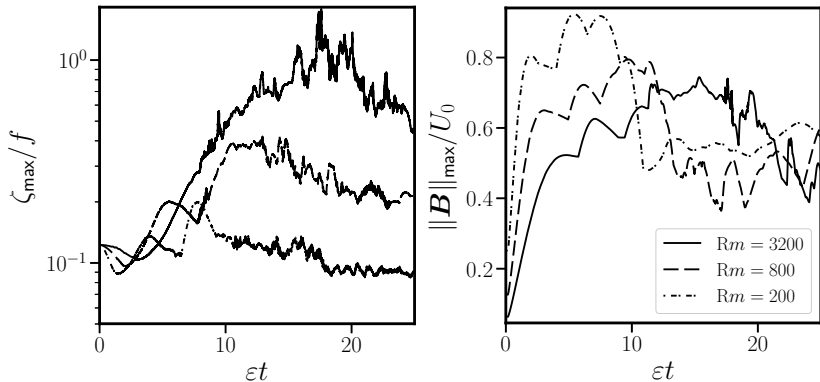
# $j_z(\mathbf{x}, 25)$ at $\text{Rm} = 3200$



# $\delta(\mathbf{x}, 25)$ at $\text{Rm} = 3200$



Evolution of the **Rossby number** (left), and **maximum horizontal magnetic field scaled by the maximum flow speed**  $U_0$  (right).



- The growth of  $\zeta$  is caused by the **magnetic Lorentz force** and **closely correlates** with  $j_z$ .
- The **actual gain**  $\|B\|_{\max}/U_0$  **decreases** with  $Rm$ .

# Conclusions (1/2)

- The concept of **balance** is especially useful in deducing *imbalance*, e.g. *inertia–gravity waves*, in complex nonlinear flows.
- **Contour Advection** can be used to efficiently study a broad range of idealised geophysical and astrophysical flows.
- **Contour Advection** is several orders of magnitude more efficient — for the same accuracy — than the **pseudo-spectral method**.
- A **non-hydrostatic** shallow-water model can be derived simply by vertically averaging, **assuming only** that the horizontal velocity (and **magnetic**) fields are **depth independent**.
- Non-hydrostatic effects **limit** the range of frequencies associated with inertia–gravity waves, **and also limit** their excitation in turbulent flows.

## Conclusions (2/2)

- 3D non-hydrostatic **rotating stratified flows** remain close to balance for Rossby numbers  $< \mathcal{O}(1)$ .
- The balance **goes beyond** quasi-geostrophic, **which is simply hydrostatic and geostrophic**. Even **ageostrophic** motions may be dominantly balanced.
- Magnetic fields **break PV conservation**: they generally **take the twist out of vorticity**.
- Shallow-water MHD flows **nonetheless enjoy a form of balance, with weak horizontal divergence**.
- Decreasing **Rossby deformation lengths**  $L_D = \sqrt{gH}/f$  **increases** the **destructive impact** of a magnetic field on vortex evolution.